UCI-HEP-TR-2014-04, IPPP/14/61, DCPT/14/122

Scattering of Dark Particles with Light Mediators

Davison E. Soper

Institute of Theoretical Science
University of Oregon
Eugene, OR 97403-5203, USA

Michael Spannowsky and Chris J. Wallace

Institute for Particle Physics Phenomenology
Department of Physics
Durham University
Durham CH1 3LE, United Kingdom

Tim M. P. Tait

Department of Physics
University of California, Irvine
Irvine, CA 92697, USA

arXiv:1407.2623v1 [hep-ph] 9 Jul 2014

Abstract

We present a treatment of the high energy scattering of dark Dirac fermions from nuclei, mediated by the exchange of a light vector boson. The dark fermions are produced by proton-nucleus interactions in a fixed target and, after traversing shielding that screens out strongly interacting products, appear similarly to neutrino neutral current scattering in a detector. Using the Fermilab experiment E613 as an example, we place limits on a secluded dark matter scenario. Visible scattering in the detector includes both the familiar regime of large momentum transfer to the nucleus (Q^2) described by deeply inelastic scattering, as well as small Q^2 kinematics described by the exchanged vector mediator fluctuating into a quark-antiquark pair whose interaction with the nucleus is described by a saturation model. We find that the improved description of the low Q^2 scattering leads to important corrections, resulting in more robust constraints in a regime where a description entirely in terms of deeply inelastic scattering cannot be trusted.

I. INTRODUCTION AND MOTIVATION

There is compelling evidence that most of the mass in the Universe is in the form of nonbaryonic dark particles. And yet, the identity of this dark matter (DM) remains elusive. Among the many proposed candidates, weakly-interacting massive particles (WIMPs) are the most popular, due to the fact that their abundance in the Universe can be explained by virtue of their being thermal relics provided they have weak scale masses and couplings [1].

One possibility is that the dark matter particles do not interact with ordinary matter strictly by the weak force. Rather, they may be able to exchange particles that interact with quarks or gluons. In this case, the relevant couplings would have to be small. Such particles could potentially be discovered by any of three methods. First, dark matter particles in locations in our galaxy where they are especially abundant could annihilate to form baryonic matter and, eventually, photons that might be detected (indirect detection). Second, dark matter particles in the halo of our galaxy might interact with nuclei in a detector on earth and this interaction might be observable (direct detection). Third, dark matter particles might be created in hadron collisons at an accelerator (accelerator production). If this happens often enough at a colliding beam accelerator such as the Large Hadron Collider, one might discover these events by looking, for example, for a missing energy signal. Alternatively, one might create dark matter particles in hadron collisions with nuclei in a fixed target and detect them through their interactions with nuclei in a suitable detector.

Currently, the best constraints on dark particles interacting with quarks come from a mixture of searches for direct detection and accelerator production. In a direct detection experiment, a particle χ with mass m_χ and velocity v_χ interacts with a nucleus in the detector and one looks for the nuclear recoil, where the typical magnitude of $v_\chi \simeq 10^{-3}$ is determined by the gravitational potential of the Galaxy. If m_χ is not large enough, the momentum $m_\chi v_\chi$ will not be large enough to create an observable nuclear recoil [2–5]. For this reason, the current generation of direct detection experiments have not been sensitive to dark matter particles with $m_\chi \lesssim 5$ GeV. However, these limits may improve in experiments using specialized detection techniques (e.g. based on measurements of ionization yield) [6, 7]. As a result, the best bounds on hadronic interactions for such light dark matter particles currently come from accelerator production at colliders [8–18], particularly for the case in which the particles mediating these interactions are heavy compared to the momentum transfer of the production process.

Of special interest are models in which the dark sector particles that mediate the interactions between the χ and standard model particles are not heavy but rather light, in some cases even lighter than the χ particles. This is the secluded scenario of Refs. [19, 20]. If the dark matter particles χ are themselves light enough so that they escape from direct detection experiments, a promising way to look for them is at fixed target experiments [20, 21] where a beam of protons strike a target to produce a beam of χ particles which are sufficiently weakly interacting so as to pass through shielding (as do neutrinos) where they can eventually be detected via their rare scattering with the nuclei comprising a detector. The advantage of a fixed target experiment over a colliding beam experiment is the higher luminosity that a fixed target experiment can offer, a key factor when searching for extremely rare production processes. In particular, we focus on the Fermilab beam dump experiment E613, which utilized a 400 GeV incoming proton beam on a tungsten target. Future high energy beam dump experiments could potentially extend the reach of E613 [22].

We employ a very simple model for the dark sector of the theory consisting of a single

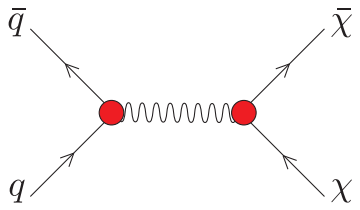

FIG. 1: Feynman diagram for direct production of χ particles from $p\,A$ collisions.

Dirac fermion dark matter particle χ and a light vector particle V, which couples to both χ particles as well as quarks. We refer to V as the dark vector boson. The relevant interactions are

$$\mathcal{L}_{\rm I} = V_\mu \left(g_{q\bar{q}v} \sum_q \bar{q}\gamma^\mu q + g_{\chi\bar{\chi}v}\, \bar{\chi}\gamma^\mu \chi \right) . \tag{1}$$

This framework is similar to a "dark photon" model, in which V picks up interactions to the Standard Model through kinetic mixing with hyper-charge [23], but differs in that it has universal charges for the quarks and is agnostic concerning the coupling to leptons. We discuss the dark photon case in more detail below, but it is worth noting here that for the regions of parameter space of interest to us, 1 MeV $< m_\chi <$ 10 GeV and $m_v \sim 1$ MeV, there are much stronger constraints on a dark photon mediator from experiments with electrons on fixed targets [24, 25] than on models interacting only with quarks [26]. Thus one might consider the interaction (1) in a leptophobic model in which the light vector particles do not couple to leptons. The leptophobic model is not really intended to be taken as a realistic model for the dark sector, but is a convenient framework to explore the degree to which non-perturbative QCD plays a role in describing how χ particles scatter off of the nuclei in a detector. The high energy of the χ particles produced by E613's 400 GeV beam demands this more detailed treatment of scattering than is necessary for the low energy neutrino factories discussed in the context of a similar model in [27–29].

We will frame the discussion in terms of a dark matter search at E613 using the simple model of Eq. (1). In Section II we describe the production of dark particles at proton fixed target experiments. In Section III, we calculate the rescattering rate of produced χs in the detector, using both a deeply inelastic scattering (DIS) approach, detailed in Section IV, and a parton saturation approach, detailed in Section V. We examine the connection between the two approaches in Section VI. In Section VII, we use the results of experiment E613 to place limits on the couplings in Eq. (1) and in a closely related "minicharge" model. Finally, we present conclusions in Section VIII. Details of the kinematics are provided in an Appendix.

II. PRODUCTION OF DARK MATTER PARTICLES

When beam protons strike the tungsten target in experiment E613, they can produce $\chi\bar{\chi}$ pairs through the diagram shown in Fig. 1. We demand that one or both of the χ particles have a high energy in the lab frame. Then this is a hard process that can be reliably calculated in lowest order perturbation theory, taking the tungsten nucleus to consist of $Z = 74$ protons and $A - Z \approx 110$ neutrons, treated as non-interacting. The interactions of

Eq. (1) are implemented in Madgraph 5 [30] with the help of FeynRules [31]. The inclusive cross sections for the process

$$pp \to \bar{\chi}\chi + X \tag{2}$$

for a proton of energy E_B incident upon a proton at rest is simulated at the parton level in the Monte Carlo generator. In order to convert this into the number of χs or $\bar{\chi}$s produced with energy E and angle θ, we write (approximating the cross section from neutrons in the nucleus as being identical to the cross sections from protons, as is approximately true in our model (1))

$$\frac{dN}{dE\,d\theta} = A\,\frac{d\sigma(pp \to \chi\bar{\chi})}{dE\,d\theta}\,L_T\,n_T\,\mathrm{POT}\ , \tag{3}$$

multiplying by the length of the target L_T, the density of tungsten nuclei inside it, n_T, and the number of protons incident on the target corresponding to the data set, POT. Here the cross section is the cross section to produce either a χ or a $\bar{\chi}$.

The number of χs that actually make it to a detector further depends on the angular acceptance of the detector. The E613 detector geometry is somewhat complicated in this regard. The detector face was 3 m $\times$ 1.5 m, with the beam offset along the horizontal axis by 0.75 m. To be conservative, we assume χs must be incident within the 0.75 m radius circle centered on the beam axis, though in practice there was a larger instrumented region which could be capable of detecting additional χs with larger production angles. The produced χs are thus incident on the detector provided their production angle is less than,

$$\theta_{\max} = \frac{0.75\ \mathrm{m}}{55.8\ \mathrm{m}} = 0.0134\ . \tag{4}$$

The number of χs per unit energy incident on the detector is then[1]

$$\frac{dN}{dE} = \int_0^{\theta_{\max}} d\theta\ \frac{dN}{dE\,d\theta}\ . \tag{5}$$

In Fig. 2, we show a plot of the calculated dN/dE divided by $g^2_{q\bar{q}v}\,g^2_{\chi\bar{\chi}v}$.

III. STRUCTURE FUNCTIONS FOR DARK MATTER SCATTERING IN THE DETECTOR

The detector is made of lead plus liquid scintillator. When a χ particle enters the detector with energy E, it can scatter from a lead nucleus. In order for the scattering to be detected, we demand that the scattering transfer at least an amount of energy E_{cut} to the nucleus. We take $E_{\mathrm{cut}} = 20$ GeV, corresponding to the minimum energy demanded by the detector to register a jet [32, 33]. Thus the expected number of events is proportional to the convolution of dN/dE from Eq. (5) with the cross section $\sigma(E, E_{\mathrm{cut}})$ for a χ particle to deposit energy greater than E_{cut} in the nucleus.

How should we calculate $\sigma(E, E_{\mathrm{cut}})$? Our process is quite analogous to deeply inelastic lepton scattering. We can take advantage of that. There is a standard analysis that allows

[1] Some dark matter particles can be lost on their way to the detector because they scatter in the rock that lies between the production point and the detector or in the iron shielding of the detector. We discuss this effect in the calculations of Sec. VII.

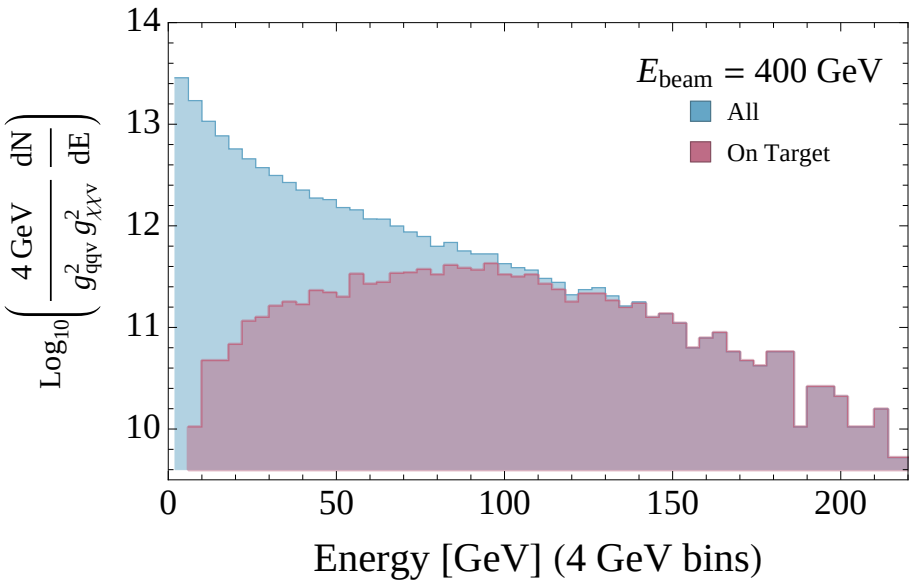

FIG. 2: Typical distribution of χ particles as a function of energy, $\frac{dN}{dE}$, divided by $g^2_{q\bar{q}v}\,g^2_{\chi\bar{\chi}v}$. The vertical scale is logarithmic. We show the distribution of all produced particles χ and $\bar{\chi}$ and the distribution of particles produced at angles that will result in their impacting the target. Many of the lowest energy dark particles are produced at wide angles and miss the detector.

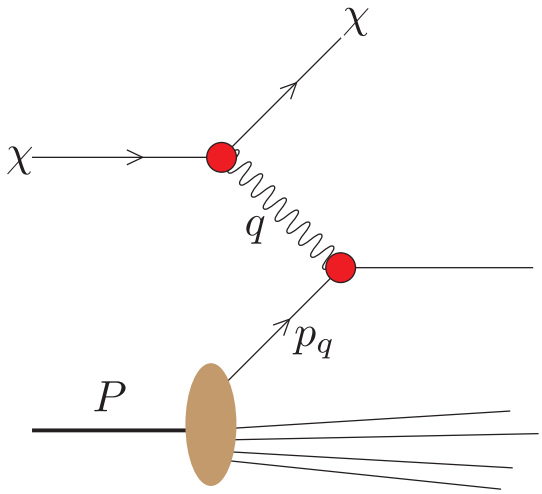

FIG. 3: Classic picture of deeply inelastic scattering from a lead nucleus, with the exchanged vector boson replaced by a massive dark vector boson that carries momentum q and interacts with a quark from the nucleus carrying momentum p_q.

us to write the cross section for χ scattering from the nucleus via vector boson exchange in terms of two structure functions, $F_{\rm T}$ and $F_{\rm L}$. In this section, we apply this standard analysis to χ scattering, using variables that are convenient for our present purposes. Although this analysis substantially simplifies the problem, it does not tell us what the structure functions $F_{\rm T}$ and $F_{\rm L}$ are. We will examine two rather different models for the structure functions in

the following two sections.

The χ particle exchanges a virtual dark vector boson with the nucleus, as depicted in Fig. 3. The χ particle has momentum p_χ before the scattering and momentum p'_χ after the scattering. The dark vector boson carries spacelike momentum $q = p_\chi - p'_\chi$. One defines $Q^2 = -q^2$ so that $Q^2 > 0$. We define ν to be the energy of the vector boson in the nucleus rest frame. Thus the cut on the energy delivered to the nucleus is a cut $\nu > E_{\rm cut}$. We let P be the momentum of the nucleus before the scattering and M be its mass. Normally, $(P+q)^2 > M^2$, so that the scattering breaks up the nucleus. We define the Bjorken scaling variable $x_{\rm bj}$ by

$$x_{\rm bj} = \frac{Q^2}{2M\nu} \ . \tag{6}$$

We use the mass M of the nucleus here. If we were to consider the nucleus as consisting of A independent nucleons, then we might instead use $Ax_{\rm bj} = Q^2/(2m_p\nu)$.

Using lowest order perturbation theory in the interactions of the vector boson and using Lorentz invariance, parity invariance, and current conservation for the strong interactions, the differential cross section has the form familiar from deeply inelastic lepton scattering:

$$d\sigma = \frac{1}{4M[E^2 - m_\chi^2]^{1/2}} \, (2\pi)^{-3} d^4p'_\chi \ \delta({p'_\chi}^2 - m_\chi^2) \, \frac{g^2_{\chi\bar\chi v} L^{\mu\nu} \ 4\pi g^2_{q\bar q v} W_{\mu\nu}}{(q^2 - m_v^2)^2} \ , \tag{7}$$

where $L^{\mu\nu}$ is

$$L^{\mu\nu} = 4p^\mu_\chi p^\nu_\chi - 2(p^\mu_\chi q^\nu + q^\mu p^\nu_\chi) + q^2 g^{\mu\nu} \tag{8}$$

and $W_{\mu\nu}$ is the hadronic matrix element of the quark currents to which the vector particle couples, not including the coupling $g^2_{q\bar q v}$ but including a conventional factor $1/(4\pi)$,

$$W_{\mu\nu} = \frac{1}{4\pi} \sum_X \langle P|J_\mu(0)|X\rangle\langle X|J_\nu(0)|P\rangle (2\pi)^4 \delta(P + q - p_X) \ . \tag{9}$$

With the use of Eq. (A19) in Appendix A, this is

$$d\sigma = \frac{g^2_{\chi\bar\chi v} \, g^2_{q\bar q v}}{16\pi M} \, \frac{d\nu \, dQ^2}{E^2 - m_\chi^2} \, \frac{L^{\mu\nu} W_{\mu\nu}}{(Q^2 + m_v^2)^2} \ . \tag{10}$$

We use ν and Q^2 as integration variables instead of the components of p'_χ. The kinematics impose limits on ν and Q^2, which we derive in Appendix A. Defining

$$\mu^2(\nu) = \frac{m_\chi^2 \nu^2}{[E(E-\nu) - m_\chi^2] + \sqrt{[E(E-\nu) - m_\chi^2]^2 - m_\chi^2 \nu^2}} \tag{11}$$

from Eq. (A13), the limits are (Eqs. (A11), (A17), and (A18))

$$\begin{aligned} E_{\rm cut} < \nu &< E - m_\chi \ , \\ 2\mu^2(\nu) < Q^2 &< 4[E(E-\nu) - m_\chi^2] - 2\mu^2(\nu) \ , \\ Q^2 &< 2M\nu \ . \end{aligned} \tag{12}$$

Now we can write $W_{\mu\nu}$ in terms of standard structure functions,

$$W^{\mu\nu} = C^{\mu\nu}_{\rm T} F_{\rm T}(x_{\rm bj}, Q^2) + C^{\mu\nu}_{\rm L} F_{\rm L}(x_{\rm bj}, Q^2) \ , \tag{13}$$

where

$$
\begin{aligned}
C_{\rm T}^{\mu\nu} &= -g^{\mu\nu} + \frac{q^\mu q^\nu}{q^2} + \frac{2x_{\rm bj}}{P\cdot q + 2x_{\rm bj}M^2}\left(P^\mu - \frac{P\cdot q}{q^2}\,q^\mu\right)\left(P^\nu - \frac{P\cdot q}{q^2}\,q^\nu\right)\ , \\
C_{\rm L}^{\mu\nu} &= \frac{1}{P\cdot q + 2x_{\rm bj}M^2}\left(P^\mu - \frac{P\cdot q}{q^2}\,q^\mu\right)\left(P^\nu - \frac{P\cdot q}{q^2}\,q^\nu\right)\ .
\end{aligned}
\tag{14}
$$

Notice that $C_{\rm T}^{\mu\nu}q_\nu = C_{\rm L}^{\mu\nu}q_\nu = 0$ and that $C_{\rm T}^{\mu\nu}a_\nu = 0$ for any vector a in the P-q plane while $C_{\rm L}^{\mu\nu}a_\nu = 0$ for any vector orthogonal to P and q. Thus $C_{\rm T}$ corresponds to the exchange of transversely polarized virtual vector bosons while $C_{\rm L}$ corresponds to the exchange of longitudinally polarized virtual vector bosons. The structure functions $F_{\rm T}$ and $F_{\rm L}$ are related to the standard structure functions F_1 and F_2 by $F_{\rm T} = F_1$ and $F_{\rm L} = (1 + 2x_{\rm bj}M^2/P\cdot q)F_2 - 2x_{\rm bj}F_1$.

We can thus write the cross section in terms of structure functions as

$$
d\sigma = \frac{g_{\chi\chi v}^2\, g_{qqv}^2}{16\pi M}\,\frac{d\nu\, dQ^2}{E^2 - m_\chi^2}\,\frac{1}{(Q^2+m_v^2)^2}\left[C_{\rm T}^{\mu\nu}L_{\mu\nu}\,F_{\rm T}(x_{\rm bj},Q^2) + C_{\rm L}^{\mu\nu}L_{\mu\nu}\,F_{\rm L}(x_{\rm bj},Q^2)\right]\ . \tag{15}
$$

One finds

$$
\begin{aligned}
C_{\rm T}^{\mu\nu}L_{\mu\nu} &= \frac{Q^2(2E-\nu)^2}{\nu^2+Q^2} + Q^2 - 4m_\chi^2\ , \\
C_{\rm L}^{\mu\nu}L_{\mu\nu} &= M\nu\,\frac{4E(E-\nu) - Q^2}{\nu^2+Q^2}\ .
\end{aligned}
\tag{16}
$$

Thus

$$
\begin{aligned}
d\sigma = \frac{g_{\chi\chi v}^2\, g_{qqv}^2}{16\pi}\,\frac{d\nu\, dQ^2}{E^2 - m_\chi^2}\,\frac{\nu}{(Q^2+m_v^2)^2}\Bigg\{ &\left[\frac{(2E-\nu)^2}{\nu^2+Q^2} + \frac{Q^2-4m_\chi^2}{Q^2}\right]2x_{\rm bj}F_{\rm T}(x_{\rm bj},Q^2) \\
&+ \frac{4E(E-\nu)-Q^2}{\nu^2+Q^2}\,F_{\rm L}(x_{\rm bj},Q^2)\Bigg\}\ .
\end{aligned}
\tag{17}
$$

The cross section that we want, $\sigma(E, E_{\rm cut})$, is then this $d\sigma$ integrated over $\nu > E_{\rm cut}$, taking into account the kinematic constraints (12). This result is exact within the approximation of considering single vector boson exchange, but, of course, we need to be able to calculate $F_{\rm T}$ and $F_{\rm L}$. We explore this in the following two sections.

IV. DIS MODEL

One way is to approach this as deeply inelastic scattering, as depicted in Fig. 3. The χ exchanges a virtual V that is absorbed by a quark in the nucleus. If Q^2 is large, there is a short distance interaction in which the vector boson interacts with a quark or gluon in the nucleus. There are also long range interactions, both in the initial state and in the final state. For an inclusive cross section like that considered here, the final state interactions do not affect the cross section. The initial state interactions do affect the cross section, but they can be factored into parton distribution functions. The short distance interaction can be calculated perturbatively. Thus $F_{\rm T}$ and $F_{\rm L}$ are written as a convolution of parton distribution functions with the partonic structure functions $\hat{F}_{\rm T}$ and $\hat{F}_{\rm L}$.

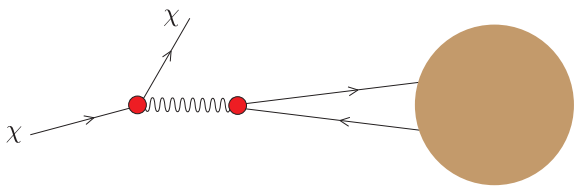

FIG. 4: Dipole picture for a χ particle scattering from a nucleus.

We will work at lowest order in perturbation theory for $\hat{F}_{\rm T}$ and $\hat{F}_{\rm L}$. At lowest order, the contributions from the gluon parton distribution function vanish for both $\hat{F}_{\rm L} = 0$ and $\hat{F}_{\rm T}$. For quarks at lowest order, $\hat{F}_{\rm L} = 0$ and $\hat{F}_{\rm T}$ is simply a delta function that sets the quark momentum fraction equal to $x_{\rm bj}$. (There would be a squared charge, $g^2_{q\bar{q}v}$, but we have already factored that out of the hadronic matrix element.) That is, $F_{\rm L} = 0$ and

$$F_{\rm T} = \frac{1}{2x_{\rm bj}} \sum_q x_{\rm bj} f_{q/A}(x_{\rm bj}, Q^2) \; . \tag{18}$$

Here we sum over flavors of quarks and antiquarks, $q = {\rm u}, \bar{\rm u}, {\rm d}, \bar{\rm d}, {\rm s}, \bar{\rm s}$ under our assumption that the mediator particle v couples equally to all the flavors. (However, we have omitted charm and bottom quarks here since the corresponding parton distribution functions are small.) We have multiplied and divided by $x_{\rm bj}$ so that one factor is $x_{\rm bj} f_{q/A}(x_{\rm bj}, Q^2)$, which is relatively insensitive to $x_{\rm bj}$ at small $x_{\rm bj}$. We note that the parton distributions here are the distributions in the nucleus A. The distribution of partons in a nucleus may be related approximately to the distribution of partons in a proton. For instance, if A is a nucleus with baryon number A and charge Z then

$$f_{{\rm u}/A}(x_{\rm bj}, Q^2) dx_{\rm bj} \approx [Z f_{{\rm u}/p}(Ax_{\rm bj}, Q^2) + (A - Z) f_{{\rm d}/p}(Ax_{\rm bj}, Q^2)] d(Ax_{\rm bj}) \; . \tag{19}$$

That is

$$f_{{\rm u}/A}(x_{\rm bj}, Q^2) \approx AZ f_{{\rm u}/p}(Ax_{\rm bj}, Q^2) + A(A - Z) f_{{\rm d}/p}(Ax_{\rm bj}, Q^2) \; . \tag{20}$$

Note that there are two factors of A or Z here. However, we use parton distribution functions for the nucleus provided at leading order by Hirai-Kumano-Nagai (HKNlo) [34], rather than this approximate formula.

Thus in the DIS model we have

$$d\sigma = \frac{g^2_{\chi\chi v}\, g^2_{qqv}}{16\pi} \frac{d\nu\, dQ^2}{E^2 - m^2_\chi} \frac{\nu}{(Q^2 + m^2_v)^2} \left[\frac{(2E - \nu)^2}{\nu^2 + Q^2} + \frac{Q^2 - 4m^2_\chi}{Q^2} \right] \sum_q x_{\rm bj} f_{q/A}(x_{\rm bj}, Q^2) \; . \tag{21}$$

This approximation for the cross section should work well as long as Q^2 is large, say larger than a few GeV^2. However, our numerical studies indicate that a good part of the cross section can come from the integration region in which $Q^2 < 1$ GeV^2. For that region, we need another model.

V. SATURATION MODEL

There is another model available that should be useful for smaller values of Q^2 and large values of ν. In this model, we view the interaction in the rest frame of the nucleus, as

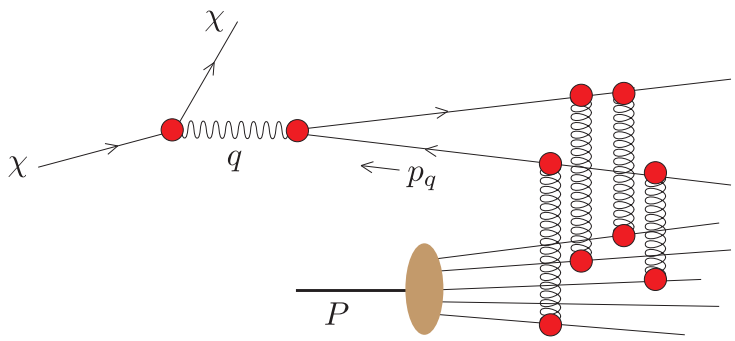

FIG. 5: The dipole created by the dark vector boson interacts with the nucleus via gluon exchange.

illustrated in Fig. 4. The dark vector boson, carrying a large momentum, splits into a quark-antiquark pair. Each of the quark and antiquark also carry a large momentum as they move towards the nucleus. Thus they form a color dipole that can interact with the nucleus. The dipole interacts with the nucleus via gluon exchange, as illustrated in Fig. 5. We will model this interaction.

To motivate the model, it is helpful to examine the kinematics of the interaction in a little detail. We work in the rest frame of the nucleus and align the negative z-axis with the momentum $\vec{q}$ of the dark vector boson. Then, defining $q^\pm = (q^0 \pm q^3)/\sqrt{2}$, we have $q^- \approx \sqrt{2}\nu$ and $q^+ \approx -2^{-3/2}Q^2/\nu$. Thus in this frame q^- is large and q^+ is small. In the Feynman diagram in Fig. 5, the dark vector boson couples to a quark propagator with momentum p_q, as in Fig. 3. We can estimate that p_q^- is large while p_q^+ is small. Imagine writing the quark propagator in coordinate space, with the quark traveling through a space-time separation Δx between the point where it interacts with a gluon from the nucleus and the point where it couples to the dark vector boson. Since $p_q \cdot \Delta x = p_q^+ \Delta x^- + p_q^- \Delta x^+ + p_q^\perp \cdot \Delta x^\perp$, we conclude that typically Δx^- is large while Δx^+ is small. That is, the quark moves a long way in the minus direction. In fact, an estimate for p_q^+ is $p_q^+ \approx 2^{-3/2}Q^2/\nu$, so that an estimate for a typical range in the minus direction is $\Delta x^- = 2^{5/2}\pi\,\nu/Q^2$. Assuming that the first interaction of the quark with a gluon is inside the nucleus, this accounting puts the interaction of the quark with the dark vector boson well outside the nucleus when ν is large and Q^2 is not large.

This physical picture, depicted in Fig. 4, seems at first to be completely different from the DIS picture of the previous section. Yet, if ν is very large and also Q^2 is large, both pictures can be correct and we can arrive at two ways of approximating the same cross section. The difference in the pictures arises from the difference of reference frames. The DIS picture is most easily derived in a reference frame in which the nucleus has a large momentum along the positive z-axis. The dipole picture of this cross section is most easily derived in the rest frame of the nucleus, with the dark vector boson having a large momentum along the negative z-axis.

We now need a model for F_T and F_L in the picture in which the dark vector boson turns into a quark-antiquark pair. The model, known as the saturation model, comes from the work of Nikolaev and Zakharov [35], Golec-Biernat and Wüsthoff [36, 37], and Mueller [38]. There is an extensive literature on the subject [39–49]. We will follow mostly Ref. [48] and will incorporate some refinements introduced by Bartels, Golec-Biernat, and Kowalski [49].

When Q^2 is small, the longitudinal structure function F_L is small compared to $2x_\mathrm{bj}F_\mathrm{T}$

since an on-shell massless vector boson does not have longitudinal polarizations. (For an analysis of $F_{\rm L}$ in the saturation picture, see ref. [50].) Thus we simply approximate $F_{\rm L}$ by zero in the saturation model, as we did in the DIS model. This leaves $F_{\rm T}$. The result [48] in the saturation model for $F_{\rm T}$ is

$$2x_{\rm bj}F_{\rm T} = \frac{1}{4\pi}\sum_f \frac{24Q^2}{(2\pi)^3}\int d\boldsymbol{b}\int d\boldsymbol{\Delta}\ \frac{G(\sqrt{Q^2+\Lambda_\rho^2}\,\Delta)}{\Delta^2}\,\Xi(\boldsymbol{b},\boldsymbol{\Delta})\ . \tag{22}$$

Here one sums over quark flavors $f = \{u, d, s\}$ and the parameter Λ_ρ is discussed below. We integrate over a two dimensional vector $\boldsymbol{b}$ and a two dimensional vector $\boldsymbol{\Delta}$. The picture as outlined above is that the dark vector boson splits into a q-$\bar{q}$ pair, both with a large momentum in the direction of the dark vector boson momentum q. When this q-$\bar{q}$ pair reaches the nucleus, the quark is at transverse position $\boldsymbol{b} + \boldsymbol{\Delta}/2$ and the antiquark is a position $\boldsymbol{b} - \boldsymbol{\Delta}/2$.

The function $G(\sqrt{Q^2+\Lambda_\rho^2}\,\Delta)/\Delta^2$ represents the squared wave function for the q-$\bar{q}$ pair, integrated over the fraction α of the longitudinal momentum of the pair that is carried by the quark. The function $G(z)$ is

$$G(z) = \int_0^1 d\alpha\ [1-2\alpha(1-\alpha)]\left[\sqrt{\alpha(1-\alpha)}\,z\,K_1(\sqrt{\alpha(1-\alpha)}z)\right]^2 . \tag{23}$$

Here $K_1(x)$ is the modified Bessel function of order 1, equal to $-dK_0(x)/dx$. The function $G(z)$ equals $2/3$ for $z = 0$. It behaves like $8/[3z^2]$ for $z \to \infty$. Thus a rough approximation to it is

$$G(z) \approx \frac{2}{3[1+z^2/4]}\ . \tag{24}$$

This approximation is good to about 15% for all values of z.

We take the argument of G to be $z = \sqrt{Q^2+\Lambda_\rho^2}\,\Delta$. The perturbative calculation gives just $Q\Delta$. That means that the spatial extent of the wave function is of order $\Delta \sim 1/Q$. That should be right for large Q. But for small Q, we expect that the q and $\bar{q}$ exchange gluons so as to bind themselves into one or more mesons – predominantly a single ρ meson. The ρ meson has a size, which we can denote by $1/\Lambda_\rho$. To represent this non-perturbative effect, it seems sensible to replace $Q\Delta$ by $\sqrt{Q^2+\Lambda_\rho^2}\,\Delta$. For the inverse radius of a ρ meson, an approximate first guess might be $\Lambda_\rho \approx 1/(1\text{ fm}) \approx 200$ MeV.

The function $\Xi(\boldsymbol{b},\boldsymbol{\Delta})$ represents the probability that the q-$\bar{q}$ pair scatters from hadron A. If Δ is not small, then this probability is approximately 1 if either the quark or the antiquark hits hadron A. But if Δ is very small, the color dipole moment of the q-$\bar{q}$ pair is small and the pair can pass right through hadron A without scattering. (This effect is known as *color transparency*). This suggests the following model (from Mueller [38] and Golec-Biernat and Wüsthoff [36, 37]). We write[2]

$$\Xi(\boldsymbol{b},\boldsymbol{\Delta}) = 1 - e^{-\Delta^2 Q_{\rm s}^2(b)/4}\ , \tag{25}$$

where $Q_{\rm s}^2$ is the *saturation scale*. Evidently if $\Delta^2 \ll 1/Q_{\rm s}^2$ then $\Xi(\boldsymbol{b},\boldsymbol{\Delta}) \propto \Delta^2$ and the scattering probability tends to zero as Δ^2 decreases. There is no scattering because the gluon field in hadron A does not see the q-$\bar{q}$ pair.

[2] Golec-Biernat and Wüsthoff write this in the form $2\int d\boldsymbol{b}\ \Xi(\boldsymbol{b},\boldsymbol{\Delta}) = \sigma_0[1-\exp(-\Delta^2/(2R_0^2)]$, which is approximately equivalent when σ_0 and R_0 are suitably adjusted.

Before we go on to talk about the saturation scale $Q_{\rm s}^2(b)$, we should discuss Eq. (25) and its connection to unitarity and to classical optics. Define $T(\boldsymbol{b},\boldsymbol{\Delta})$ by $\Xi(\boldsymbol{b},\boldsymbol{\Delta}) = 1 - T(\boldsymbol{b},\boldsymbol{\Delta})$. We think of Ξ as the probability for the dipole to be absorbed by the nucleus and we think of T as the analogue of the transmission coefficient in optics [48]. Let R_A be the radius of the nucleus. We can then determine the necessary limiting properties of the function $T(\boldsymbol{b},\boldsymbol{\Delta})$. Here we follow Ref. [48], which contains more details.

- If the dipole misses the nucleus, i.e. $|\boldsymbol{b}| > R_A + \Delta/2$, then $\Xi(\boldsymbol{b},\boldsymbol{\Delta})$ must be zero, therefore $T(\boldsymbol{b},\boldsymbol{\Delta}) = 1$.

- If the quark and the antiquark that make up the dipole are separated from each other by zero distance then, since it is a color singlet object, it simply passes through the nucleus. Therefore, $T(\boldsymbol{b},\boldsymbol{\Delta}) = 1$ for $\Delta = 0$.

- For small Δ, the probability for the dipole to interact with the nucleus should be proportional to the square of the color dipole moment of the dipole: $T(\boldsymbol{b},\boldsymbol{\Delta}) \propto \Delta^2$. We need Δ^2 here because in the cut Feynman diagram for the process the dipole must exchange at least two gluons with the nucleus.

- For small Δ, we can calculate the coefficient of Δ^2 in T using QCD perturbation theory.

- $T(\boldsymbol{b},\boldsymbol{\Delta}) \approx 0$ for large dipoles (large Δ), when $|\boldsymbol{b}| < R_A$. That is, a large, strongly interacting dipole cannot pass through the nucleus leaving it intact.

To calculate the coefficient of Δ^2 in T, we recognize that the probability that the gluon field does see the q-$\bar{q}$ pair depends not only on how small the color dipole moment is but also on how strong the gluon field is. Thus it is not surprizing that the saturation scale $Q_{\rm s}^2(b)$ in Eq. (25) is proportional to the density of gluons in the nucleus:

$$Q_{\rm s}^2(b) = \frac{2\pi^2\alpha_{\rm s}(\mu^2)}{3}\, xG(x,\mu^2)\,\phi(b)\ . \tag{26}$$

Here $\phi(b)$ is modeled as a geometrical quantity that tells how the gluons are spread in the transverse separation from the center of the nucleus:

$$\phi(b) = \frac{3}{2\pi R_A^3}\,\sqrt{R_A^2 - b^2}\,\Theta(b^2 < R_A^2)\ . \tag{27}$$

The function $\phi(b)$ is normalized to $\int d\boldsymbol{b}\,\phi(b) = 1$. The function $G(x,\mu^2)$ is the gluon distribution function in the nucleus. We again employ the HKNlo distribution for lead, which is defined such that the total gluon distribution for the nucleus is given by $G(x,\mu^2) = A\,G_{\rm HKN}(A\,x_{\rm bj},\mu^2)$, which we insert in place of $G(x,\mu^2)$ in equation (26).

We need to set μ^2 in $\alpha_{\rm s}(\mu^2)$ and $xG(x,\mu^2)$ and we need to set x in $xG(x,\mu^2)$. We follow the form of the choices of Bartels, Golec-Biernat, and Kowalski [49]. For the scale μ^2, we take

$$\mu^2 = \frac{C}{\Delta^2} + \mu_0^2\ . \tag{28}$$

The choice of a constant divided by Δ^2 is sensible in the perturbative regime of small Δ^2. However, for large Δ^2 we do not want μ^2 to be arbitrarily small. Thus we add a constant,

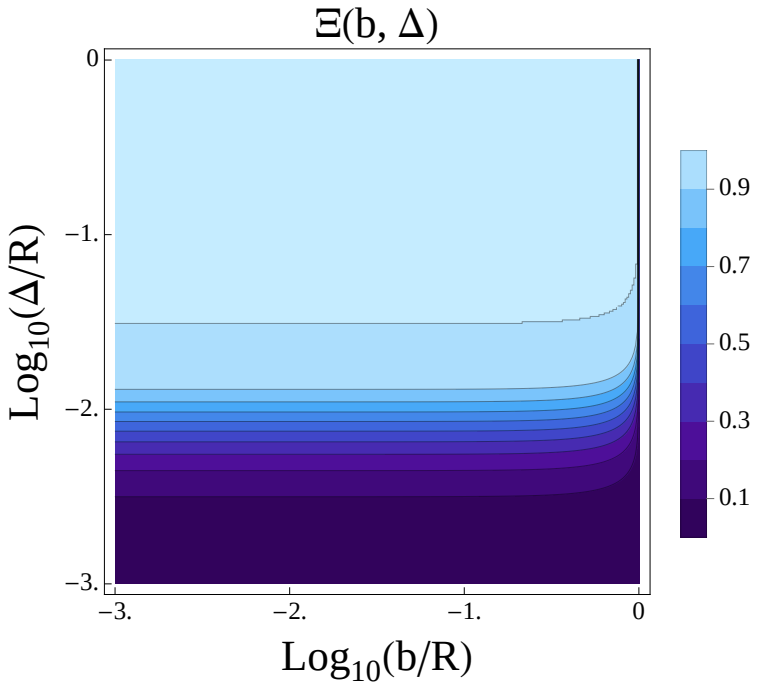

FIG. 6: The function $\Xi(\boldsymbol{b}, \boldsymbol{\Delta})$ as a function of $|\boldsymbol{b}|/R$ and $|\boldsymbol{\Delta}|/R$ where R is the radius of the lead nucleus. We calculate $\Xi(\boldsymbol{b}, \boldsymbol{\Delta})$ using Eqs. (25), (26), and (27) with parameters given in Eqs. (28) and (29) and using HKNlo parton distributions for the distribution of gluons in a lead nucleus, with $x = 10^{-4}$ and $Q^2 = 1$ GeV^2.

μ_0^2 to C/Δ^2. We find a reasonable fit for $C = 6.00$ and $\mu_0^2 = 2.0$ GeV^2. For the momentum fraction variable in the gluon distribution, we take

$$x = \frac{Q^2 + 4m_{\rm q}^2}{2M\nu} \ . \tag{29}$$

This is $x_{\rm bj}$ when Q^2 is not too small. But for very small Q^2, we do not want x to be arbitrarily small. Thus we add a small mass term, $4m_{\rm q}^2$, to Q^2. This is in the same spirit as our adjustment of the argument of $G(z)$ in Eq. (22). Following Ref. [49], we take $m_{\rm q} = 140$ MeV.

We see that there is some QCD theory and some modeling in the net formula for Ξ. The resulting function $\Xi(\boldsymbol{b}, \boldsymbol{\Delta})$ is illustrated in Fig. 6. We can perhaps appreciate from the figure that the model dependence is less than one might have thought. For $|\boldsymbol{\Delta}| > R/10$, $\Xi(\boldsymbol{b}, \boldsymbol{\Delta})$ is very close to 1 for $|\boldsymbol{b}| < R$. When we get to $|\boldsymbol{b}| \approx R$, Ξ drops very quickly to zero. The value $\Xi \approx 1$ is nonperturbative, but it is not really model dependent because 1 is the largest that Ξ could be. For $|\boldsymbol{\Delta}| < R/10$, the behavior of $\Xi(\boldsymbol{b}, \boldsymbol{\Delta})$ is not so trivial. However, this region is perturbative, so we have some control over the theory. In part, the shape is determined by the function $\phi(b)$ from Eq. (27). This part of the formula for Ξ is simply a model for the distribution of gluons. The model is that the density of gluons is uniform throughout the nucleus. Thus there is some model dependence, but the model dependence is not too large.

There is more model dependence in the function $G(\sqrt{Q^2 + \Lambda_\rho^2}\,\Delta)/\Delta^2$ in Eq. (23). This function is calculated using lowest order perturbation theory, so it should be accurate for large Q^2 and, correspondingly, small Δ. For small Q^2 it simply represents a plausible model.

VI. CONNECTION BETWEEN THE DIS AND SATURATION MODELS

In Eq. (22), we can try to take the large Q^2 limit of $x_{\rm bj}F_{\rm T}$ by taking the large Q^2 limit under the integration over $\boldsymbol{\Delta}$. In this limit, the argument, $\sqrt{Q^2+\Lambda_\rho^2}\,\Delta$, of the function G becomes just $Q\Delta$. Then for large $Q\Delta$ we have $G(Q\Delta) \sim 8/[3Q^2\Delta^2]$, as we noted earlier. We need to enforce that $Q\Delta$ is large inside the integration over $\boldsymbol{\Delta}$ and we do that in a crude way by inserting a factor $\Theta(\Delta > a/Q)$ for some constant a. This gives the approximation

$$2x_{\rm bj}F_{\rm T} \approx \sum_f \frac{2}{\pi^4}\int d\boldsymbol{b}\int d\boldsymbol{\Delta}\;\frac{\Theta(\Delta>a/Q)}{\Delta^4}\,\Xi(\boldsymbol{b},\boldsymbol{\Delta})\;. \tag{30}$$

This matches with our DIS formula Eq. (18) if we identify

$$x\,f_{q/A}(x,Q^2) = \frac{1}{\pi^4}\int d\boldsymbol{b}\int d\boldsymbol{\Delta}\;\frac{\Theta(\Delta>a/Q)}{\Delta^4}\,\Xi(\boldsymbol{b},\boldsymbol{\Delta})\;. \tag{31}$$

There is a factor of 2 in this formula that results from suming over flavors f in Eq. (30) and over flavors and antiflavors in Eq. (18). The right hand side of this equation has some x dependence because the gluon distribution that appears in the exponent in Ξ depends on x. It is independent of the choice of quark flavor or antiflavor $q \in \{\mathrm{u},\bar{\mathrm{u}},\mathrm{d},\bar{\mathrm{d}},\mathrm{s},\bar{\mathrm{s}}\}$.

There is a more direct approach to this, which was obtained in Ref. [48]. One starts directly with the operator definition of the parton distribution functions, $f_{q/A}(x,\mu^2)$, and analyzes the operator matrix element using the dipole picture. The operator matrix element requires ultraviolet renormalization, to eliminate a divergence from small Δ in the integration over $\boldsymbol{\Delta}$. To match the standard $\overline{\rm MS}$ definition of parton distribution functions, one should use dimensional regularization and an appropriate pole subtraction. However, one can obtain the same result at one loop order with a simple cut. The result of this analysis is Eq. (31) with

$$a = 2e^{1/6-\gamma_{\rm E}} \approx 1.32657\;. \tag{32}$$

Eq. (31) is based on lowest order perturbation theory for the wave function of the quark dipole, so one expects that it should begin to be accurate for Q^2 large enough so that perturbation theory applies. However the formula does not properly account for DGLAP evolution, so the result should begin to fail for very large Q^2. In Fig. 7, we test how well this relationship works by ploting $Axf_{q/A}(Ax,Q^2)$ versus $\log_{10}(Ax)$ for a few values of Q^2. We see that the approximation in Eq. (31) is only moderately successful at $Q^2 = 2$ GeV^2, but that it works quite well for $Q^2 = 10$ GeV^2. By $Q^2 = 50$ GeV^2, it is still working quite well but is beginning to fail.

VII. APPLICATION TO SCATTERING OF DARK MATTER

We have studied the scattering of dark Dirac fermions through a vector mediated interaction with quarks. This amounts to a neutrino–like neutral current event, with the added theoretical interest of having no heavy electroweak boson to regulate the momentum transfer of the interaction. In this section we shall apply this formalism to a model of dark matter.

Continuing from Section II, with the scattering cross sections now in hand, it is straightforward to calculate the number of events expected in the detector. We first calculate the

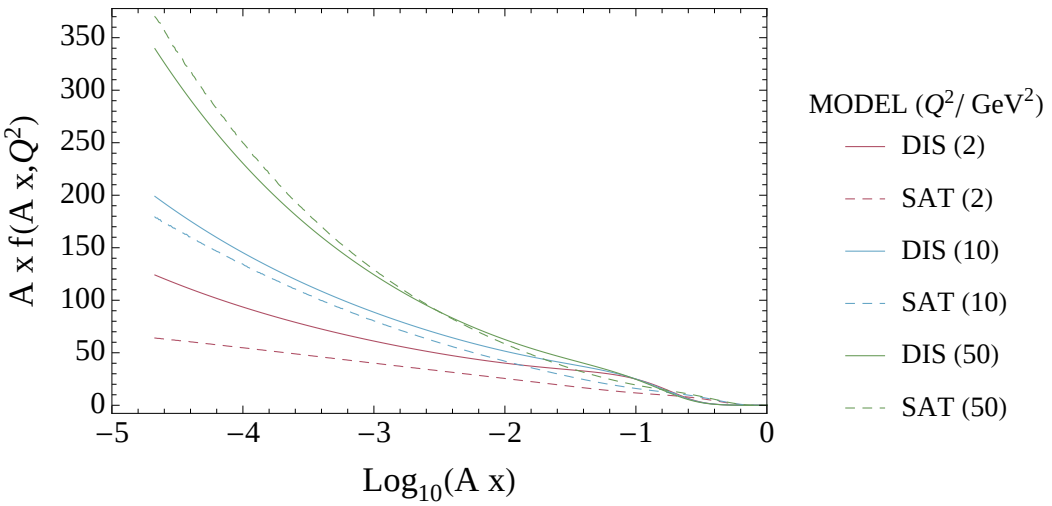

FIG. 7: The parton distribution function $f_{q/A}(x, Q^2)$ for ū quarks in a uranium nucleus according to the HKNlo parton distributions [34] used in this paper compared to the same distribution in the saturation model, Eq. (31). We plot $Axf_{q/A}(Ax, Q^2)$ versus $\log_{10}(Ax)$ for $Q^2 = 2$ GeV^2, 10 GeV^2, and 50 GeV^2.

mean free path of the propagating dark particle,

$$\lambda = \frac{1}{\rho_A \, \sigma(\chi N \to \chi N)}, \tag{33}$$

where ρ_A is the number density of nuclei and $\sigma(\chi N \to \chi N)$ is the nuclear scattering cross section. The mean free path enters into the rescattering probability,

$$P = \int_0^L dx \, \frac{1}{\lambda} e^{-\frac{x}{\lambda}} = 1 - e^{-\frac{L}{\lambda}}. \tag{34}$$

The final number of events expected in the detector is,

$$N_{\text{det.}} = \int dE \; (1 - P_{\text{shielding}}(E)) \times P_{\text{detector}}(E) \times \frac{dN}{dE}, \tag{35}$$

where dN/dE is defined in equation (5). For scattering in the shielded region, composed of ~ 15 m of iron, we impose an arbitrary 1 GeV cut on the required energy transfer to prevent divergence of the deep inelastic cross section. We note that in practice, for the small values of the couplings that we can constrain, the probability of rescattering in shielding is extremely small, such that practically no scattering occurs. Further, since the probability of any given dark particle scattering is so low, one does not need to account for the degradation of the beam along the length of the detector, and can approximate the scattering probability as simply $P \sim L/\lambda$. A fully realistic treatment would include multiple rescatterings, including low energy scatters that degrade the energy of incoming particles. This is not necessary for our purposes, which are adequately modeled by a single scattering event per dark particle.

Using equation (35) and data provided by the experimental collaboration [32, 33] (and interpreted as below in [51]), we may constrain our model. The E613 experiment delivered 1.8×10^{17} protons on target (POT), and estimate that at most 100 detected events per 10^{17}

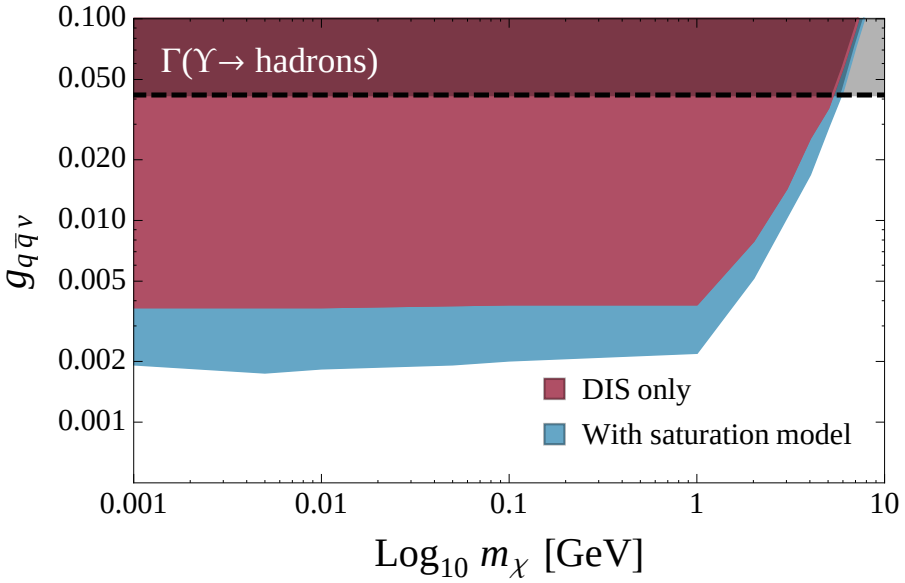

FIG. 8: Exclusion limits for the leptophobic model described in the text, with $g_{\chi\bar{\chi}v} = 1$ and a mediator mass of 1 MeV. Also plotted is the region excluded by the study of Υ decays from [26].

POT represent muonless neutral current events at 90% C.L. Thus, we exclude couplings where the number of expected detector events, $N_\chi > 180$.

The result of this analysis as applied to the model (1) is shown in Fig. 8, with the mediator mass set to 1 MeV and the mediator–dark particle coupling fixed to unity. The two colored regions in the plot correspond to the scattering models described in Sections IV and V. The "DIS only" region cuts off integration of the cross section for $Q^2 < 1$ GeV^2, applying the scattering picture of Section IV. The region labeled "With saturation model" applies the same formalism, but additionally includes the dipole scattering mechanism described in Section V for the $Q^2 < 1$ GeV^2 region, resulting in a substantial improvement of the constraint. Also plotted is a mapping of the constraint on a leptophobic U(1) gauge boson, which couples to baryon number. Several constraints on such a model are described in [26], the strongest of which (plotted) arises from the contribution of the new boson to the decay width of Υ mesons into hadronic final states. While we emphasize that this is a toy model, very similar models are of considerable phenomenological interest, and apt to be studied at existing fixed target facilities [29].

As another concrete example to demonstrate the impact of our formalism, we consider a "minicharged" particle scenario [52], which is realized as the limit in which the mediator is a massless $U(1)$ vector boson which mixes kinetically with hypercharge [23, 52–55]. The dark sector matter (the Dirac fermion) that is charged under the additional U(1) interacts with the standard model only through this mixing, which is parametrized via the mixing angle, κ, in the gauge invariant Lagrangian term $\mathcal{L} \supset -\frac{\kappa}{2} F^{\mu\nu} X_{\mu\nu}$, where $F^{\mu\nu}$ and $X^{\mu\nu}$ are respectively the field strength tensors of the SM and dark U(1) gauge groups.

One can diagonalize the kinetic term in the Lagrangian with a field redefinition, the result of which is to induce electromagnetic interactions with the dark particles, which have an effective "minicharge", $\epsilon = \kappa g_{\rm h}/e$, where $g_{\rm h}$ is the hidden photon-dark fermion coupling and e is the electromagnetic coupling constant. Then the cross section for both production and scattering scale with ϵ^2. For our scenario involving quarks, the appropriate quark charges

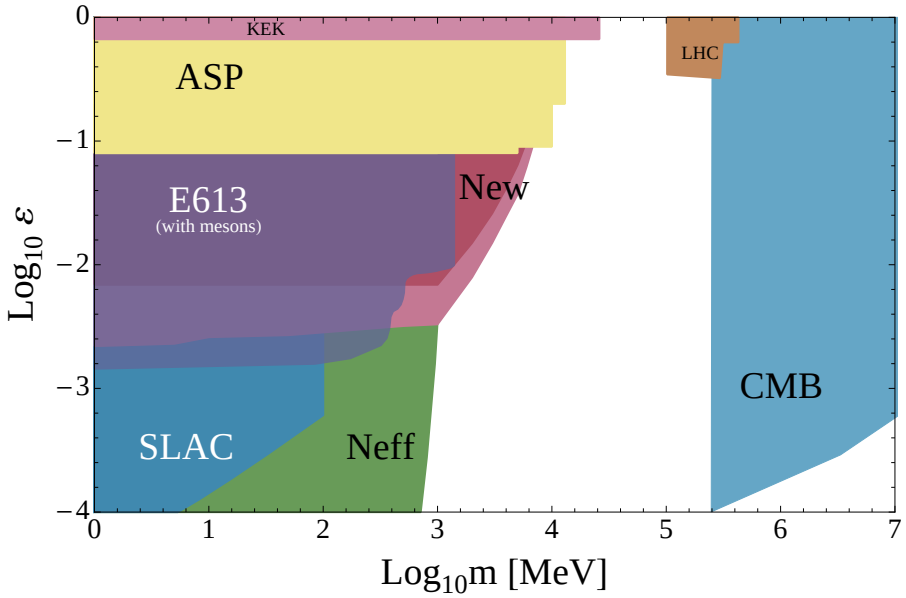

FIG. 9: Exclusion limits for minicharged particles in the MeV to GeV mass regime, including the results of this analysis. Other constraints are shown, arising from colliders [56], a SLAC beam dump [57], the LHC [58], CMB [59, 60] and recent work on the number of light species, $N_{\rm eff}$ [61].

must be included in the cross section, such that the coupling of the mediator to the nucleus is correctly modeled as proceeding via mixing with the photon. The exclusion limits on the minicharge ϵ are shown in Fig. 9. It is worth noting that the constraint from the effective number of light particle species, $N_{\rm eff}$, is strong but subject to astrophysical uncertainties that make terrestrial collider based studies worthwhile.

In Fig. 10, we compare (only) the constraints on the mini-charge model previously derived from E613 [51] with those derived in this work, in the plane of the mini-charged particle mass and ϵ. The results from our analysis using only the deeply inelastic scattering regime are shown as the red dashed line, whereas the inclusion of the low $Q^2 < 1$ GeV^2 regime via dipole scattering leads to the solid red line. A large improvement in the strength of the bound from the improved treatment of the low transfer scattering is evident. The previous constraint [51] is shown as the shaded region, and shows a marked transition in the strength of the bound on ϵ by about an order of magnitude as the particle mass crosses a few hundred MeV. This sharp transition is the result of dark particle production through meson decay, which switches off around 500 MeV, leaving Drell-Yan production of the dark particles to dominate. We have not included this production mechanism in our bound, as it is model-dependent and tangential to our goal of an improved description of the χ-nucleus scattering cross section. A more appropriate comparison of the impact of our improved computations is to the blue dashed curve, which extrapolates the previous bound by extending the Drell-Yan-only limit to lower masses. Of course, the actual bound on the mini-charged model at low mass would be better represented by including the χ production from meson decay together with our improved treatment of the scattering, though this is beyond the scope of this work. Clearly, fixed target experiments are a fertile ground for testing this class of models.

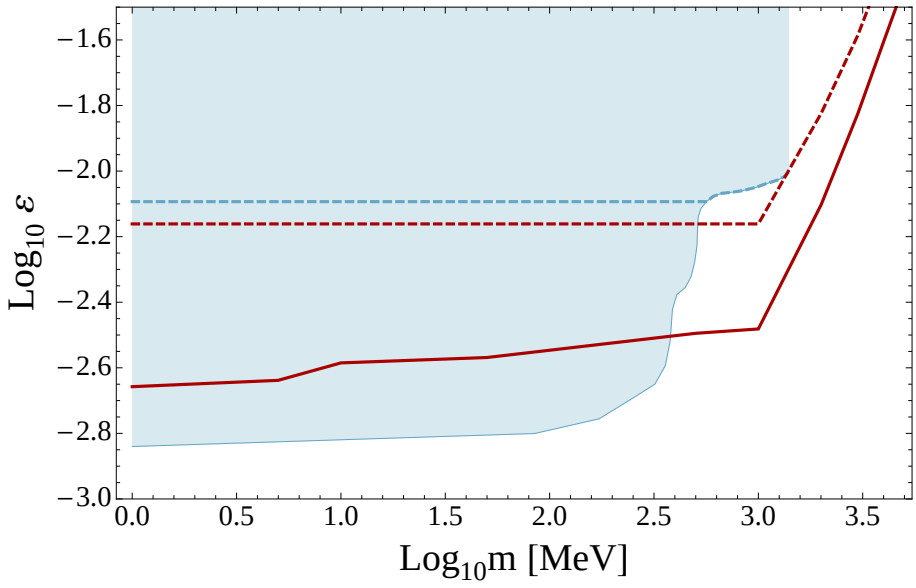

FIG. 10: The minicharge constraints arising only from the E613 experiment. See text for details.

VIII. CONCLUSIONS

We have investigated the detection of dark Dirac fermions in the context of the E613 beam dump experiment. The model employed gives rise to neutral current scattering, but in the absence of a heavy electroweak gauge boson to mediate the interaction. We studied the deep inelastic scattering in the detector in detail, and introduced a model valid at the low Q^2 values that become important in the absence of a heavy mediator to regulate the $1/Q^4$ behavior of the cross section. By including the effects of scattering at $Q^2 < 1$ GeV^2 with a well theoretically motivated dipole model, we substantially improve upon constraints calculated using parton-level deep inelastic scattering alone. This could be especially relevant for new particle searches at future high energy beam dump facilities, which would allow access to regions of low Q^2 and small Bjorken-x.

Acknowledgements

DES thanks Francesco Hautmann for helpful conversations. CJW thanks ITP Heidelberg for hospitality while performing some of this work, Joerg Jaeckel for providing questions and Céline Bœhm for now ancient but very useful conversations. MS acknowledges the hospitality of the Aspen Center for Physics while part of this work was finished. MS and CJW thank Lucian Harland-Lang for enlightenment regarding nuclear parton distribution functions. All authors are grateful to Paolo Gondolo for the suggestion to consider extending an earlier analysis of MINOS to old beam dump experiments. The research of TMPT is supported in part by NSF grant PHY-1316792 and by the University of California, Irvine through a Chancellor's Fellowship. The research of DES was supported in part by the United States Department of Energy.

Appendix A: Kinematics

In this appendix, we present some of the details for the cross section for scattering a dark spin 1/2 particle, χ, with momentum p_χ, from a hadron A with momentum P. The hadron can be a nucleus. The dark particle has mass m_χ while the hadron has mass M. The dark particle mass may be of order 1 GeV or it may be smaller. The dark particle energy in the hadron rest frame, which we call E, is large compared to 1 GeV. We will introduce two different models for the scattering cross section.

In the hadron rest frame, we write the components of P and p_χ as

$$P = (M, 0, 0, 0) , \tag{A1}$$

$$p_\chi = (E, 0, 0, k) , \tag{A2}$$

where $k = \sqrt{E^2 - m_\chi^2}$. The final state χ has 4-momentum

$$p'_\chi = (E - \nu, k' \sin\theta\cos\phi, k' \sin\theta \sin\phi, k' \cos\theta) , \tag{A3}$$

where

$$k' = \sqrt{(E-\nu)^2 - m_\chi^2} . \tag{A4}$$

We suppose that the χ in the final state is not observed. Thus we will integrate over p'_χ.

The momentum transfer is

$$q = p_\chi - p'_\chi \tag{A5}$$

and is characterized by the energy transfer ν,

$$q \cdot P = M\nu , \tag{A6}$$

and by the invariant

$$Q^2 = -q^2 \tag{A7}$$

with $Q^2 > 0$. In terms of the final state χ momentum,

$$Q^2 = 2E(E-\nu) - 2kk'\cos\theta - 2m_\chi^2 . \tag{A8}$$

We define

$$x_{\rm bj} = \frac{Q^2}{2M\nu} . \tag{A9}$$

Note that $x_{\rm bj} \leq 1$. Also note that when A is a nucleus of baryon number A, one often defines a scaled $x_{\rm bj}$ equal to $AQ^2/(2M\nu)$. We do not do that here. However, we note that the ultimate limit on $x_{\rm bj}$ is $x_{\rm bj} \leq 1$, but the practical limit beyond which the cross section is very small is $x_{\rm bj} \leq 1/A$.

We will integrate over Q^2 and ν and will need the integration limits. Begin with ν. We will impose a cut

$$\nu > E_{\rm cut} \quad . \tag{A10}$$

That is, we wish to calculate the cross section for the process when at least a certain amount of energy $E_{\rm cut}$ is delivered to the hadron. Also Eq. (A4) and $k'^2 > 0$ gives $\nu < E - m_\chi$. Thus the integration range for ν is

$$E_{\rm cut} < \nu < E - m_\chi . \tag{A11}$$

Next, we need the limits on Q^2 at fixed ν. Define a function $\mu^2(\nu)$ by

$$kk' = E(E-\nu) - \mu^2(\nu) - m_\chi^2 \ . \tag{A12}$$

Then

$$\mu^2(\nu) = \frac{m_\chi^2 \nu^2}{[E(E-\nu) - m_\chi^2] + \sqrt{[E(E-\nu) - m_\chi^2]^2 - m_\chi^2 \nu^2}} \ . \tag{A13}$$

Then Q^2 has a simple form in terms of $\mu^2(\nu)$,

$$Q^2 = 2[E(E-\nu) - m_\chi^2][1 - \cos\theta] + 2\mu^2(\nu)\cos\theta \ . \tag{A14}$$

One boundary of the integration region is forward scattering, $\cos\theta = 1$. On this boundary we have

$$Q^2 = 2\mu^2(\nu) \ , \qquad\qquad \cos\theta = 1 \ . \tag{A15}$$

The other boundary of the integration region is at $\cos\theta = -1$. There, we have

$$Q^2 = 4[E(E-\nu) - m_\chi^2] - 2\mu^2(\nu) \ , \qquad\qquad \cos\theta = -1 \ . \tag{A16}$$

For small m_χ, this is $Q^2 \approx 4E(E-\nu)$ with small corrections. Put together, the inequalities $-1 < \cos\theta < 1$ lead to

$$2\mu^2(\nu) < Q^2 < 4[E(E-\nu) - m_\chi^2] - 2\mu^2(\nu) \ . \tag{A17}$$

There is a separate upper bound for Q^2. The momentum q is absorbed by the hadron, giving a final state with momentum $P+q$. We need $(P+q)^2 > M^2$. This condition gives $x_{\rm bj} < 1$ or

$$Q^2 < 2M\nu \ . \tag{A18}$$

Having found the integration limits, we translate the integration over p'_χ into integration over ν and Q^2 (integrating over the azimuthal angle ϕ to give a factor 2π). We obtain,

$$\begin{aligned} d^4p'_\chi \ \delta({p'_\chi}^2 - m_\chi^2) &= \frac{k'^2 dk'}{2E'} \, d\cos\theta \, d\phi \\ &= \frac{\pi}{2\sqrt{E^2 - m_\chi^2}} \, d\nu \, dQ^2 \ . \end{aligned} \tag{A19}$$

where $E' = E - \nu$ and k' is given by Eq. (A4).

We will introduce two different models for the structure functions, and in particular for $F_{\rm T}$. We will simply state the results of these models. However, if we want to examine the physics behind the models, it is convenient to use choose our reference frame wisely. We note that $F_{\rm T}$ and $F_{\rm L}$ depend only on q and P. Thus we should choose a frame in which q and P are simple. We choose a frame in which both q and P have no transverse components and in which q has a positive 3-component. Additionally, we now write momentum components in $(p^+, p^-, \boldsymbol{p}^T)$ format with $p^\pm = (p^0 \pm p^3)/\sqrt{2}$. In our new frame,

$$\begin{aligned} P &= (M/\sqrt{2}, M/\sqrt{2}, \mathbf{0}) \ , \\ q &= \left(\frac{1}{\sqrt{2}} \left[\nu + \sqrt{\nu^2 + Q^2} \right], -\frac{1}{\sqrt{2}} \frac{Q^2}{\nu + \sqrt{\nu^2 + Q^2}}, \mathbf{0} \right) \end{aligned} \tag{A20}$$

In the kinematic region important for this paper, $Q^2 \ll \nu^2$, so that

$$q \approx \left(\sqrt{2}\,\nu, -\frac{Q^2}{2\sqrt{2}\,\nu}, \mathbf{0} \right) \quad . \tag{A21}$$

Thus $q^+ \gg q^-$.

[1] G. Bertone, D. Hooper and J. Silk, Phys. Rept. **405**, 279 (2005) [hep-ph/0404175].

[2] D. S. Akerib *et al.* [LUX Collaboration], arXiv:1310.8214 [astro-ph.CO].

[3] E. Aprile *et al.* [XENON100 Collaboration], arXiv:1207.5988 [astro-ph.CO].

[4] Z. Ahmed *et al.* [CDMS Collaboration], Phys. Rev. D **81**, 042002 (2010) [arXiv:0907.1438 [astro-ph.GA]].

[5] G. Angloher, M. Bauer, I. Bavykina, A. Bento, C. Bucci, C. Ciemniak, G. Deuter and F. von Feilitzsch *et al.*, Eur. Phys. J. C **72**, 1971 (2012) [arXiv:1109.0702 [astro-ph.CO]].

[6] R. Essig, A. Manalaysay, J. Mardon, P. Sorensen and T. Volansky, Phys. Rev. Lett. **109**, 021301 (2012) [arXiv:1206.2644 [astro-ph.CO]].

[7] P. Cushman, C. Galbiati, D. N. McKinsey, H. Robertson, T. M. P. Tait, D. Bauer, A. Borgland and B. Cabrera *et al.*, arXiv:1310.8327 [hep-ex].

[8] J. Goodman, M. Ibe, A. Rajaraman, W. Shepherd, T. M. P. Tait and H. -B. Yu, Phys. Lett. B **695**, 185 (2011) [arXiv:1005.1286 [hep-ph]].

[9] Y. Bai, P. J. Fox and R. Harnik, JHEP **1012**, 048 (2010) [arXiv:1005.3797 [hep-ph]].

[10] J. Goodman, M. Ibe, A. Rajaraman, W. Shepherd, T. M. P. Tait and H. -B. Yu, Phys. Rev. D **82**, 116010 (2010) [arXiv:1008.1783 [hep-ph]].

[11] P. J. Fox, R. Harnik, J. Kopp and Y. Tsai, Phys. Rev. D **85**, 056011 (2012) [arXiv:1109.4398 [hep-ph]].

[12] A. Rajaraman, W. Shepherd, T. M. P. Tait and A. M. Wijangco, Phys. Rev. D **84**, 095013 (2011) [arXiv:1108.1196 [hep-ph]].

[13] Y. Bai and T. M. P. Tait, arXiv:1208.4361 [hep-ph].

[14] T. Aaltonen *et al.* [CDF Collaboration], Phys. Rev. Lett. **108**, 211804 (2012) [arXiv:1203.0742 [hep-ex]].

[15] K. Cheung, P. -Y. Tseng, Y. -L. S. Tsai and T. -C. Yuan, JCAP **1205**, 001 (2012) [arXiv:1201.3402 [hep-ph]].

[16] S. Chatrchyan *et al.* [CMS Collaboration], arXiv:1204.0821 [hep-ex].

[17] S. Chatrchyan *et al.* [CMS Collaboration], arXiv:1206.5663 [hep-ex].

[18] . Aad *et al.* [ATLAS Collaboration], JHEP **1304**, 075 (2013) [arXiv:1210.4491 [hep-ex]].

[19] B. Batell, M. Pospelov and A. Ritz, Phys. Rev. D **79**, 115008 (2009) [arXiv:0903.0363 [hep-ph]].

[20] B. Batell, M. Pospelov and A. Ritz, Phys. Rev. D **80**, 095024 (2009) [arXiv:0906.5614 [hep-ph]].

[21] R. Essig, R. Harnik, J. Kaplan and N. Toro, Phys. Rev. D **82**, 113008 (2010) [arXiv:1008.0636 [hep-ph]].

[22] J. L. Hewett, H. Weerts, K. S. Babu, J. Butler, B. Casey, A. de Gouvea, R. Essig and Y. Grossman *et al.*, arXiv:1401.6077 [hep-ex].

[23] K. R. Dienes, C. F. Kolda and J. March-Russell, Nucl. Phys. B **492**, 104 (1997) [hep-ph/9610479]; T. G. Rizzo, Phys. Rev. D **59**, 015020 (1998) [hep-ph/9806397]; F. del Aguila, M. Masip and M. Perez-Victoria, Nucl. Phys. B **456**, 531 (1995) [hep-ph/9507455]; J. Kumar and J. D. Wells, Phys. Rev. D **74**, 115017 (2006) [hep-ph/0606183].

[24] J. D. Bjorken, R. Essig, P. Schuster and N. Toro, Phys. Rev. D **80**, 075018 (2009) [arXiv:0906.0580 [hep-ph]].

[25] B. Batell, R. Essig and Z. 'e. Surujon, arXiv:1406.2698 [hep-ph].

[26] C. D. Carone and H. Murayama, Phys. Rev. Lett. **74**, 3122 (1995) [hep-ph/9411256]; C. D. Carone and H. Murayama, Phys. Rev. D **52**, 484 (1995) [hep-ph/9501220].
[27] P. deNiverville, M. Pospelov and A. Ritz, Phys. Rev. D **84**, 075020 (2011) [arXiv:1107.4580 [hep-ph]].
[28] P. deNiverville, D. McKeen and A. Ritz, Phys. Rev. D **86**, 035022 (2012) [arXiv:1205.3499 [hep-ph]].
[29] B. Batell, P. deNiverville, D. McKeen, M. Pospelov and A. Ritz, arXiv:1405.7049 [hep-ph].
[30] J. Alwall, M. Herquet, F. Maltoni, O. Mattelaer and T. Stelzer, JHEP **1106**, 128 (2011) [arXiv:1106.0522 [hep-ph]].
[31] N. D. Christensen and C. Duhr, Comput. Phys. Commun. **180**, 1614 (2009) [arXiv:0806.4194 [hep-ph]].
[32] T. A. Romanowski, Acta Phys. Polon. B **16**, 179 (1985).
[33] M. E. Duffy, G. K. Fanourakis, R. J. Loveless, D. D. Reeder, E. S. Smith, S. Childress, C. Castoldi and G. Conforto *et al.*, Phys. Rev. D **38**, 2032 (1988).
[34] M. Hirai, S. Kumano and T. -H. Nagai, *Determination of nuclear parton distribution functions and their uncertainties in next-to-leading order*, Phys. Rev. C **76**, 065207 (2007) [INSPIRE].
[35] N. N. Nikolaev and B. G. Zakharov, *Color transparency and scaling properties of nuclear shadowing in deep inelastic scattering*, Z. Phys. C **49**, 607 (1991) [INSPIRE].
[36] K. J. Golec-Biernat and M. Wusthoff, *Saturation effects in deep inelastic scattering at low Q**2 and its implications on diffraction*, Phys. Rev. D **59**, 014017 (1998) [INSPIRE].
[37] K. J. Golec-Biernat and M. Wusthoff, *Saturation in diffractive deep inelastic scattering*, Phys. Rev. D **60**, 114023 (1999) [INSPIRE].
[38] A. H. Mueller, *Parton saturation at small x and in large nuclei*, Nucl. Phys. B **558**, 285 (1999) [INSPIRE].
[39] L. Frankfurt, A. Radyushkin and M. Strikman, *Interaction of small size wave packet with hadron target*, Phys. Rev. D **55**, 98 (1997) [INSPIRE].
[40] J. R. Forshaw, G. Kerley and G. Shaw, *Extracting the dipole cross-section from photoproduction and electroproduction total cross-section data*, Phys. Rev. D **60**, 074012 (1999) [INSPIRE].
[41] M. McDermott, L. Frankfurt, V. Guzey and M. Strikman, *Unitarity and the QCD improved dipole picture*, Eur. Phys. J. C **16**, 641 (2000) [INSPIRE].
[42] E. Gotsman, E. Levin, M. Lublinsky, U. Maor, E. Naftali and K. Tuchin, *Has HERA reached a new QCD regime?: (Summary of our view)*, J. Phys. G **27**, 2297 (2001) [INSPIRE].
[43] A. H. Mueller, *Parton saturation: An Overview*, in J.P.Blaizot and E. Iancu, eds. "QCD perspectives on hot and dense matter. Proceedings, NATO Advanced Study Institute", Cargese, France, August, 2001, hep-ph/0111244 [INSPIRE].
[44] K. J. Golec-Biernat, *Physics of parton saturation*, Acta Phys. Polon. B **35**, 3103 (2004) [INSPIRE].
[45] K. J. Golec-Biernat, *Theoretical review of diffractive phenomena*, Nucl. Phys. A **755**, 133 (2005) [INSPIRE].
[46] P. Tribedy and R. Venugopalan, *Saturation models of HERA DIS data and inclusive hadron distributions in p+p collisions at the LHC*, Nucl. Phys. A **850**, 136 (2011) [Erratum-ibid. A **859**, 185 (2011)] [INSPIRE].
[47] A. Luszczak and H. Kowalski, *Dipole model analysis of high precision HERA data*, arXiv:1312.4060 [hep-ph] [INSPIRE].
[48] F. Hautmann, D. E. Soper, *Parton distribution function for quarks in an s-channel approach*, Phys. Rev. **D75**, 074020 (2007) [INSPIRE].

[49] J. Bartels, K. J. Golec-Biernat and H. Kowalski, *A modification of the saturation model: DGLAP evolution*, Phys. Rev. D **66**, 014001 (2002) [INSPIRE].
[50] M. V. T. Machado, Eur. Phys. J. C **47** (2006) 365.
[51] Golowich, E. and Robinett, R. W. Phys. Rev. D **35**, 391 (1987).
[52] B. Holdom, Phys. Lett. B **166**, 196 (1986).
[53] L. B. Okun, Sov. Phys. JETP **56**, 502 (1982) [Zh. Eksp. Teor. Fiz. **83**, 892 (1982)].
[54] P. Galison and A. Manohar, Phys. Lett. B **136**, 279 (1984).
[55] J. Jaeckel, Frascati Phys. Ser. **56**, 172 (2012) [arXiv:1303.1821 [hep-ph]].
[56] S. Davidson, B. Campbell and D. C. Bailey, Phys. Rev. D **43**, 2314 (1991).
[57] A. A. Prinz, R. Baggs, J. Ballam, S. Ecklund, C. Fertig, J. A. Jaros, K. Kase and A. Kulikov *et al.*, Phys. Rev. Lett. **81**, 1175 (1998) [hep-ex/9804008].
[58] J. Jaeckel, M. Jankowiak and M. Spannowsky, Phys. Dark Univ. **2** (2013) 111 [arXiv:1212.3620 [hep-ph]].
[59] A. D. Dolgov, S. L. Dubovsky, G. I. Rubtsov and I. I. Tkachev, Phys. Rev. D **88**, no. 11, 117701 (2013) [arXiv:1310.2376 [hep-ph]].
[60] S. L. Dubovsky, D. S. Gorbunov and G. I. Rubtsov, JETP Lett. **79**, 1 (2004) [Pisma Zh. Eksp. Teor. Fiz. **79**, 3 (2004)] [hep-ph/0311189].
[61] H. Vogel and J. Redondo, JCAP **1402**, 029 (2014) [arXiv:1311.2600 [hep-ph]].